Supporting Information for

π-extension improves the photovoltaic performance: helical perylene diimide oligomer based three-dimensional non-fullerene acceptor

Mingliang Wu,[‡a] Ping Xia,[‡b] Huaxi Huang,[a] Zhaohang Lin,[b] Xiaoxiao You,[a] Keke Wang,[b] Huan Lu,[b] Di Wu,*[b] Jianlong Xia*[a]

[a]State Key Laboratory of Advanced Technology for Materials Synthesis and Processing, Center of Smart Materials and Devices, Wuhan University of Technology No. 122 Luoshi Road, Wuhan 430070, China

[b]School of Chemistry, Chemical Engineering and Life Science, Wuhan University of Technology No. 122 Luoshi Road, Wuhan 430070, China

[‡]These authors contributed equally to this work.

Email: D.W.(chemwd@whut.edu.cn); J.X. (jlxia@whut.edu.cn)

Table of the contents

1. General Information

All chemical reactions were conducted in oven-dried or flame-dried glassware. A homo-built flow photochemical reactor[1] was used to synthesize the **SF-4PDI2** with Au Light CEL-LB70 as the light source. All the chemicals and starting materials were purchased from commercial sources without further treatment unless specially noted. The commercially available polymer donor PTB7-Th was purchased from Solarmer Materials Int. with a MW over 40000 and a PDI of 1.8-2.0. Compounds perylene diimide,[2] monobromoperylene diimide[3] and perylene diimide dimer[4] were synthesized according to literature procedures.

^{1}H NMR and ^{13}C NMR spectra were measured on Bruker DRX 500 or Varian Mercury plus-400. MALDI-TOF Mass spectrum was measured with AB Sciex 5800. UV-Vis spectrum was recorded on Shimadzu UV-1800. Cyclic voltammograms (CVs) were obtained on CHI660E electrochemical workstation. A three-electrode one-compartment cell containing a solution of the analyte and supporting electrolyte (tetrabutylammonium, ($[NBu_4]PF_6$), 0.1M) in dry CH_2Cl_2 was utilized. A 500 μm diameter platinum-disk working electrode, a platinum-wire counter electrode, and an Ag/AgCl reference electrode were used. The atomic force microscope (AFM) images were recorded by a Dimension Icon AFM (Bruker).

Thermogravimetric analysis (TGA) was carried out on a tainstruments SDT Q-600 under a nitrogen atmosphere at a heating rate of 5 ^{o}C/min.

DFT calculations were performed by using the Gaussian 09 software package at the B3LYP/6-31G(d) level. The alky chains were replaced by hydrogen atoms to reduce the computation cost. All the optimized ground-state structures were shown to be minima by the absence of imaginary frequencies. The HOMOs and LUMOs of these two molecules were obtained by using the Multiwfn program[5] and visualized *via* the VMD package.[6]

Device fabrication: The inverted devices were fabricated with the structure of ITO/ZnO/active layer/MoO_3/Ag. The pre-patterned (sheet resistance, 15 Ω/sq) ITO-glass substrates were sequentially cleaned in ultrasonic bath with detergent (Alconox Inc.), de-ionized water, acetone and isopropanol. The oven-dried substrates were then treated by an oxygen plasma (180 W) for 5 min. The ZnO precursor solution (110 mg/mL) was prepared by dissolving 0.22 g $ZnAc_2{\cdot}2H_2O$ in 2 mL 2-methoxyethanol and 0.056 mL ethanol amine and then stirred for at least 24h before use. The solution was filtered with polyether sulfone (PES) filters. The ZnO precursor solution was spin-cast onto ITO substrate with spinning rate of 5000 rpm for 60s and the thickness was ~32 nm. The as-cast film was then annealed in ambient circumstance upon 150 ^{o}C for 60 min to form a compact ZnO layer. The blend solutions of PTB7-Th:**SF-4PDI2** mixtures were processed with o-dichlorobenzene (o-DCB) with an identical concentration of 35 mg mL^{-1}. All these solutions were heated at 60 ^{o}C and stirred overnight (or 100 ^{o}C for 3h) to obtain well-mixed blend solutions. The active layer thicknesses of these three devices were carefully optimized through spinning rate 3500 rpm. And, the spinning duration was fixed at 50s. The active layers were thermal annealed at 60 ^{o}C in glove box for 10 min to get rid of residual solvent. A MoO_3 (8 nm) layer and an Ag layer (100 nm) electrode were

sequentially deposited by thermal evaporation using a shadow mask under a vacuum of $<1.0\times10^{-4}$ pa. The effective device area, defined by the overlap region of ITO and Ag electrodes, was 0.0625 cm^2.

The *J-V* measurements were conducted under AM 1.5G illumination at 100 mW cm^{-2} using an AAA solar simulator (SP94023A-SR1, NEWPORT). The illumination intensity was calculated with a standard photovoltaic cell (91150V) which incorporated with a quartz window (1000P072). External quantum efficiency (EQE) was determined by an EQE system (Zolix, China). The film thicknesses were determined on Eoptics SE-VM Spectroscopic Ellipsometer.

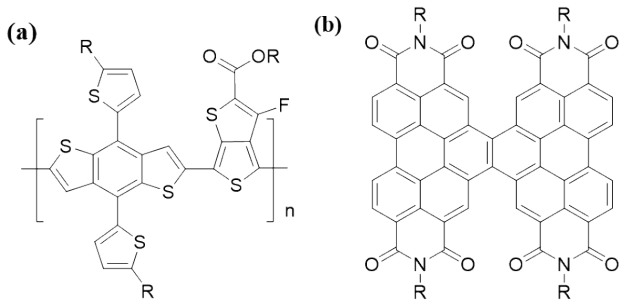

Fig. S1 Chemical structure of (a) PTB7-Th (electron donor), (b) PDI oligomer (PDI2).

2. Material Synthesis

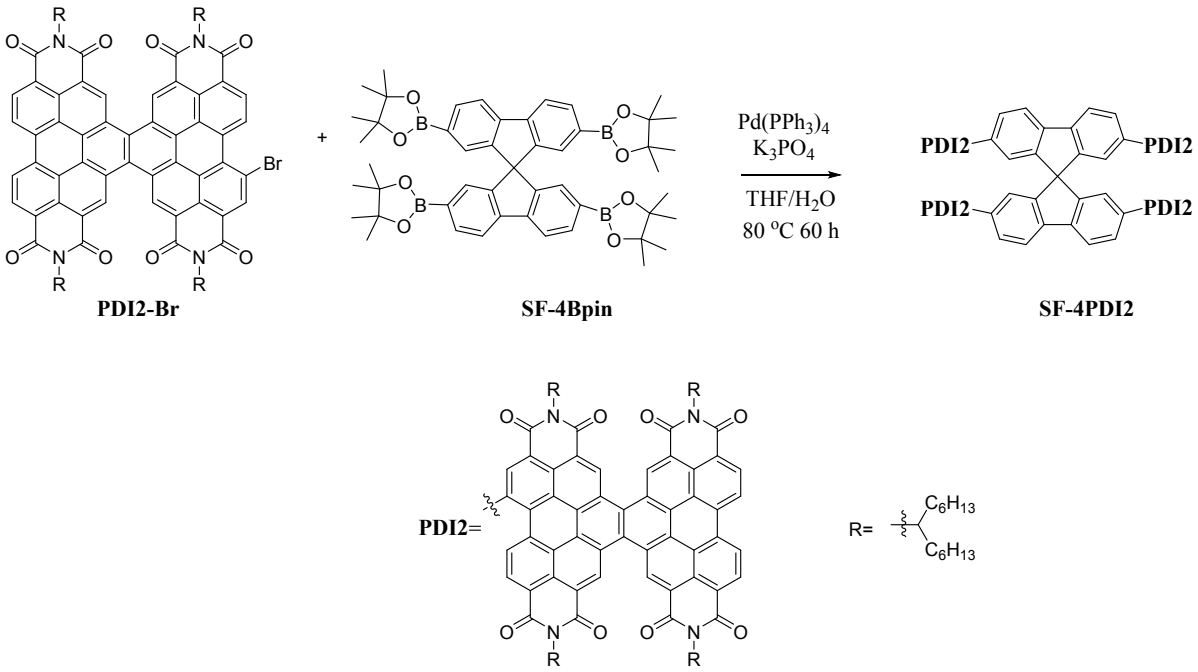

Scheme S1. Synthetic route of SF-4PDI2

A 100 ml flask was charged with $Pd(PPh_3)_4$ (100 mg, 0.086 mmol), K_3PO_4 (400 mg, 1.88 mmol), PDI2-Br (1.5 g, 0.93 mmol, 5.2 equiv) and SF-4Bpin (145 mg, 0.177 mmol, 1 equiv). The charged flask was evacuated and backfilled with nitrogen for 30 minutes. The oxygen-free THF/H_2O (V/V=4:1, 50 ml) was introducing to the flask as solvent via syringe. Then the mixture was heated to 80 °C for 60 h. The solution was then cooled to room temperature and diluted with water and dichloromethane. The combined organic layers were dried over Na_2SO_4, and evaporated under reduced pressure. And the crude solid was purified by silica gel chromatography eluted with petroleum ether/CH_2Cl_2 from 2:1 to 1:3, further recrystallization with DCM/MeOH afforded the target molecule SF-4PDI2 as dark red laminar solid (410 mg, 36%). ^{1}H NMR (400 MHz, Chloroform-*d*) δ 10.17 (d, *J* = 111.3 Hz, 17H), 9.32 (d, *J* = 117.4 Hz, 27H), 8.62 – 7.54 (m, 12H), 5.30 (s, 16H), 2.35 (s, 32H), 1.99 (s, 32H), 1.31 (s, 256H), 0.78 (s, 96H). ^{13}C NMR (101 MHz, $CDCl_3$) δ 165.14, 164.96, 164.82, 164.62, 164.09, 163.76, 163.54, 141.90, 141.38, 134.23, 134.19, 134.15, 133.97, 132.27, 131.15, 130.80, 130.72, 129.99, 127.28,

127.07, 126.99, 126.91, 126.81, 126.77, 126.72, 126.60, 126.55, 126.39, 126.29, 126.24, 126.21, 126.16, 126.11, 125.67, 124.31, 123.98, 123.84, 123.48, 123.39, 123.22, 122.47, 122.36, 55.11, 32.37, 32.34, 31.76, 29.72, 29.25, 28.99, 27.04, 26.72, 22.59, 22.41, 22.30, 14.01, 13.65, 13.58, 13.49. MALDI-TOF: $[SF\text{-}4PDI2+Na]^+$ calculated for 6451.7111; found 6451.5845.

3. Thermal Gravimetric Analysis (TGA)

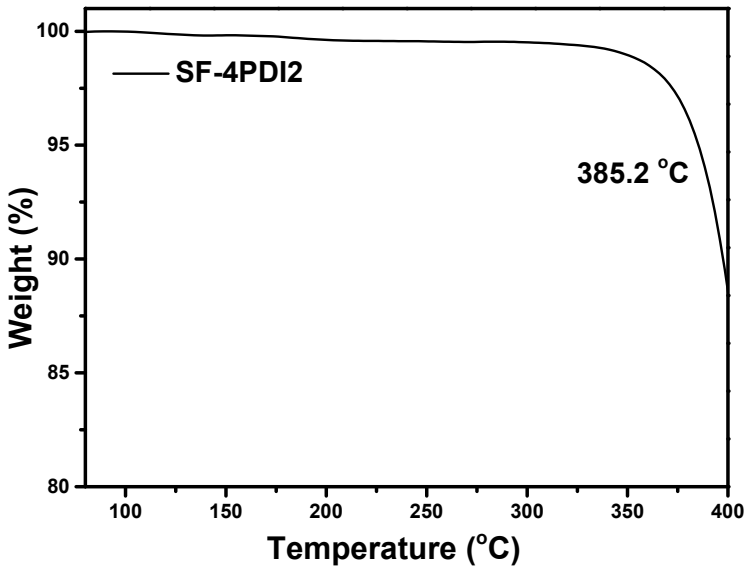

Fig. S2 Thermogravimetric analysis (TGA) result of **SF-4PDI2** with a heating rate of 5 °C/min under nitrogen.

4. DFT Calculation

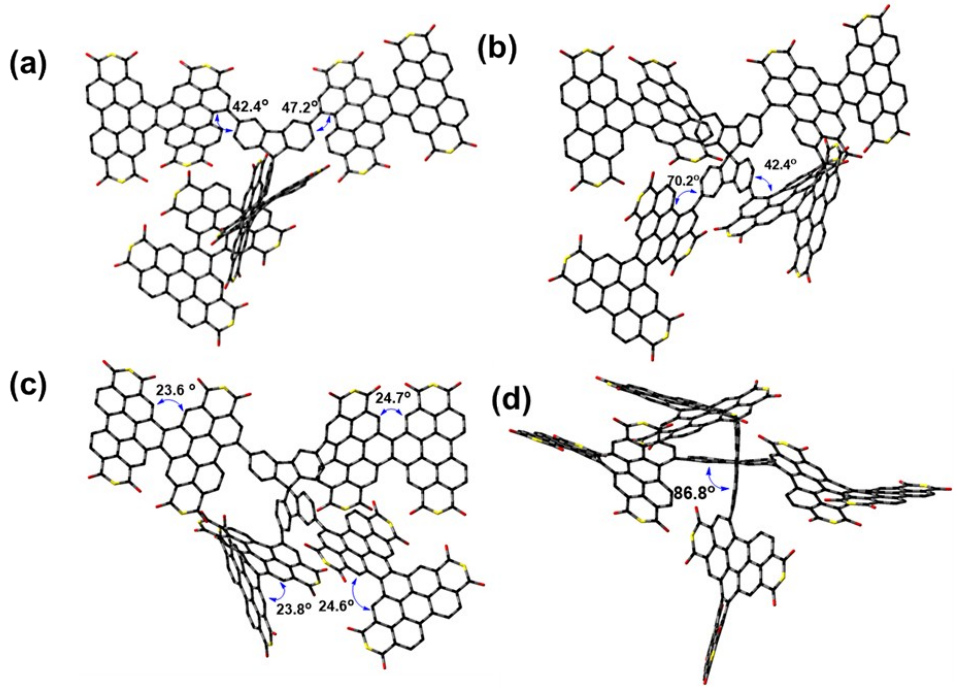

Fig. S3 DFT calculation results of **SF-4PDI2** (a, b) dihedral angles between inner PDI units and the spiro-fluorene (SF) core and (c) dihedral angles between two PDI units, (d) dihedral angles between two parts of spiro-fluorene.

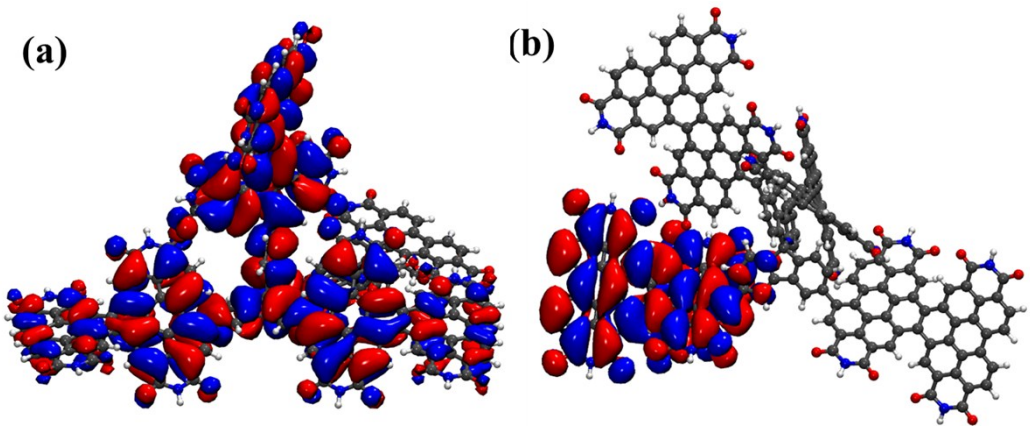

Fig. S4 DFT calculated frontier orbitals of **SF-4PDI2** (a) HOMO and (b) LUMO.

Table S1. The HOMO, LUMO Energies and their energy gap of **SF-4PDI2**.

Compound	$E_{(HOMO)}^{cal}$ / eV	$E_{(LUMO)}^{cal}$ / eV	E_{gap}^{cal} / eV
SF-4PDI2	−6.03	−3.82	2.21

5. UV-Vis in solution Cyclic Voltammograms (CVs)

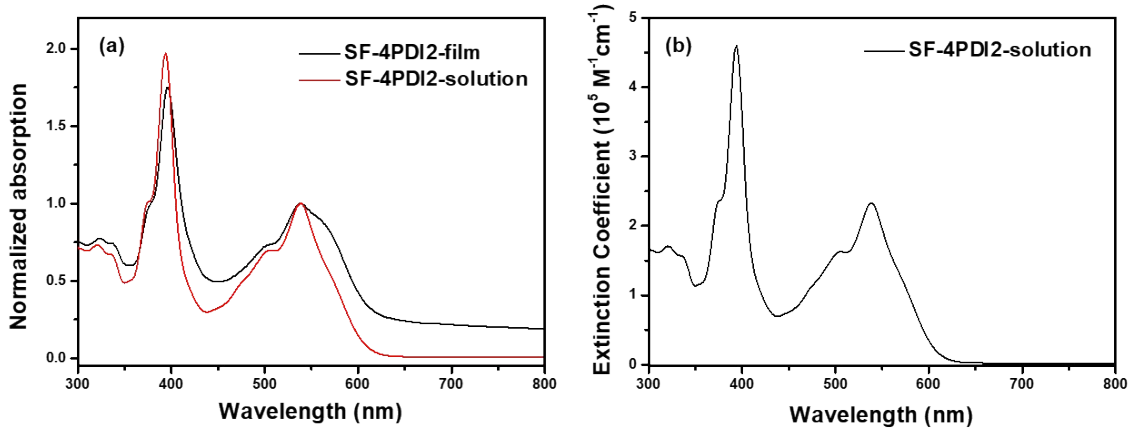

Fig. S5 (a) Normalized absorption spectra of **SF-4PDI2** film and chloroform solution, (b) UV-vis absorption spectra in chloroform solution at concentrations of 5×10^{-6} M.

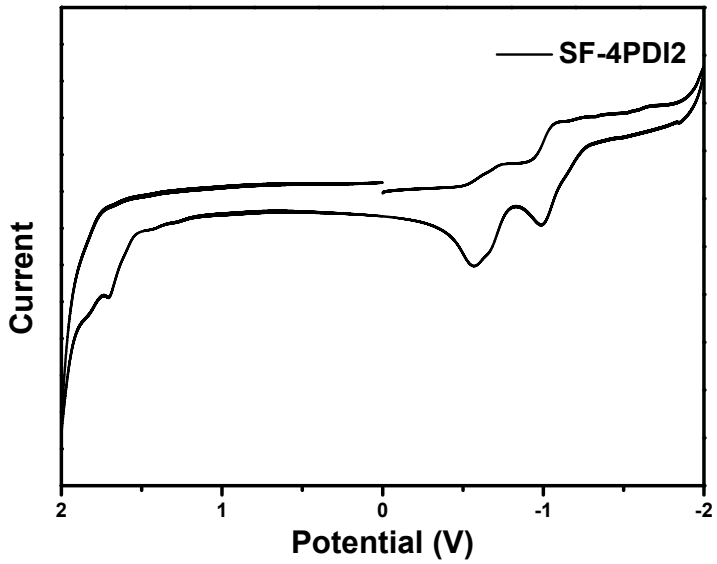

Fig. S6 Cyclic voltammograms (CVs) of **SF-4PDI2** at 100 mV/s in DCM solution.

6. The Photovoltaic Performance of the Devices

Table S2. The summary devices parameters of PTB7-Th:**SF-4PDI2** under different D/A ratio.

PTB7-Th:SF-4PDI2	V_{oc}/V	J_{sc}/mA cm^{-2}	FF/%	PCE $_{max}$/%
1:0.5	0.79	13.59	44.3	4.76
1:1.0	0.80	14.61	54.9	6.45
1:1.2	0.83	5.79	55.7	7.35
1:2.0	0.82	13.33	58.9	6.48
1:2.5	0.82	12.55	57.9	6.02

These values were obtained from five individual devices for each condition.

Table S3. The summary devices parameters of PTB7-Th:**SF-4PDI2** under different thermal annealing times.

PTB7-Th:SF-4PDI2	V_{oc}/V	J_{sc}/mA cm^{-2}	FF/%	PCE $_{max}$/%
As-cast	0.83	5.79	55.7	7.35
60 ^{o}C for 10 mins	0.82	15.65	58.6	7.69
60 ^{o}C for 20 mins	0.81	15.54	58.6	7.39
60 ^{o}C for 30 mins	0.81	15.64	54.9	6.95
60 ^{o}C for 60 mins	0.81	15.45	58.3	7.28

These values were obtained from five individual devices for each condition.

Table S4. The summary devices parameters of PTB7-Th:**SF-4PDI2** under different thermal annealing temperatures.

PTB7-Th:SF-4PDI2	V_{oc}/V	J_{sc}/mA cm^{-2}	FF/%	PCE $_{max}$/%
As-cast	0.83	5.79	55.7	7.35
60 ^{o}C for 10 mins	0.82	15.65	58.6	7.69
80 ^{o}C for 10 mins	0.82	14.99	58.3	7.20
100 ^{o}C for 10 mins	0.81	14.94	57.2	6.96
120 ^{o}C for 10 mins	0.81	15.21	57.3	7.09
140 ^{o}C for 10 mins	0.82	14.96	56.9	6.99

These values were obtained from five individual devices for each condition.

Table S5. The summary device parameters for the previous reported SF-core PDI tetramer and dimer.

Donor:Acceptor	V_{oc} (V)	J_{sc} (mA/cm^2)	FF (%)	PCE (%)	Ref.
PTB7-Th:SBF-PDI$_4$	0.86	8.82	48	3.66	7
PTB7-Th:SBF-PDI$_4$ (CN)	0.85	13.08	48	5.34	
PTB7-Th:SFPDI4	0.90±0.01	10.9±0.1	51.9±0.3	5.1±0.1	8
PTB7-Th:PDI4	0.90±0.005	13.36±0.05	56.3±0.3	6.44	9
PTB7-Th:SF-PDI4	0.87±0.01	12.00±0.54	46.0±1.1	5.01	10
PTB7-Th:SF-iPDI2 (DIO)	0.84	10.53	59.9	5.31	11
PTB7-Th:SF-iPDI4 (DIO)	0.82	11.36	50.1	4.68	
P4T2FBT:SF-PDI4 (DIO)	0.93±0.001	11.03±0.18	51.1±1.36	5.27	12
PV4T2FBT:SF-PDI4 (DIO)	0.90±0.005	12.02±0.09	54.2±1.63	5.98	
PBDB-T:BP-PDI$_4$	0.90	13.6	59.7	7.3	13
PffBT4T-2OD:SF-PDI4	0.94±0.01	8.21±0.36	50.7±4.8	4.09	10
PffBT4T-2OD:SF-PDI2	0.91±0.01	5.86±0.23	55.4±1.2	3.05	
PTB7:SpiroF-B-PDI	0.75	5.90	36	1.57	14
P3TEA:SF-PDI$_2$	1.11	13.27	64.3	9.5	15
PffBT4T-2DT:SF-PDI2	0.98±0.01	10.7±0.4	57	6.0	16
PTB7-Th:SF-PDI2	1.00±0.01	7.4±0.2	39	2.9	
P3HT:5	0.61	6.27	60	2.28	17
P3HT:6	0.61	5.92	65	2.35	
PTB7-Th: SPFPDI44 (CN)	0.90	9.27	46.84	3.91	18
PTB7-Th: SPFPDI24 (CN)	0.93	10.05	45.37	4.24	

These data were obtained from references.

7.The Integration of the EQE

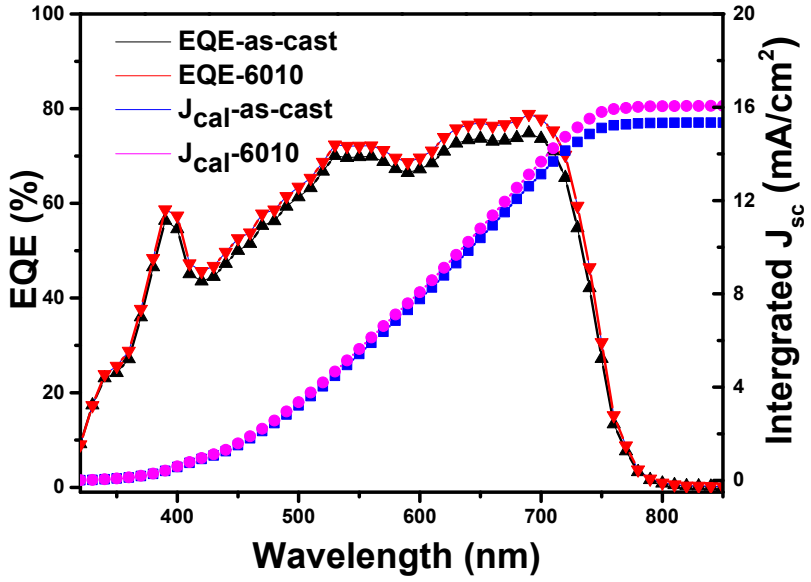

Fig. S7 The EQE for **SF-4PDI2** (as-cast, black), (annealed at 60 °C for 10 mins, red) and calculated short-circuit current density (J_{sc}) from the EQE for **SF-4PDI2** (as-cast, blue), (annealed at 60 °C for 10 mins, purple).

8. Photoluminescence Quenching Experiment

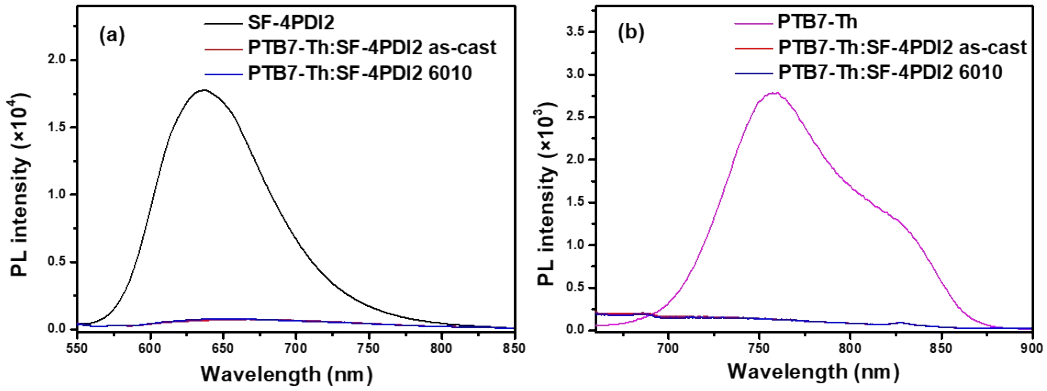

Fig. S8 The comparison profiles of photoluminescence (PL) spectra of (a) pure films of **SF-4PDI2** and blend films of PTB7-Th:**SF-4PDI2** (as-cast, 6010), (excited at 530 nm); (b) pure films of PTB7-Th and blend films of PTB7-Th:**SF-4PDI2** (as-cast, 6010), (excited at 630 nm). The 6010 films were annealed upon 60 °C in glove box for 10 mins.

Table S6. PL quenching efficiency of the neat film of donor (PTB7-Th), acceptor (SF-4PDI2) and their blend films (as-cast, annealed at 60 °C for 10 mins).

Blending films	PL Quenching efficiency (%)	
	Quenching induced by electron transfer	Quenching induced by hole transfer
PTB7-Th:SF-4PDI2 as-cast	88.91%	92.11%
PTB7-Th:SF-4PDI2-6010	89.48%	92.03%

9. The Light Density Dependent J_{sc} and V_{oc} Measurements

The dependence of J_{sc} of the devices on the illumination light density was conducted to gain insight into the exciton recombination dynamics of these devices. And the results are shown in **Figure S9**, The dependence of J_{sc} of the OSCs on the illumination intensity can be expressed as $J_{sc} \propto (P_{light})^S$. Generally, bimolecular recombination is negligible under short circuit conditions if the S value approaches 1.0 (linear relationship). As for the open circuit condition, the relationship between V_{oc} and light intensity can be described as $V_{oc} \propto nkT/q \ln(P_{light})$, where k is Boltzmann's constant, T is the temperature, and q is the elementary charge. When the fitting slope value is ≥2 kT/q, then the device mainly suffers monomolecular recombination (mainly for trap-assist recombination).

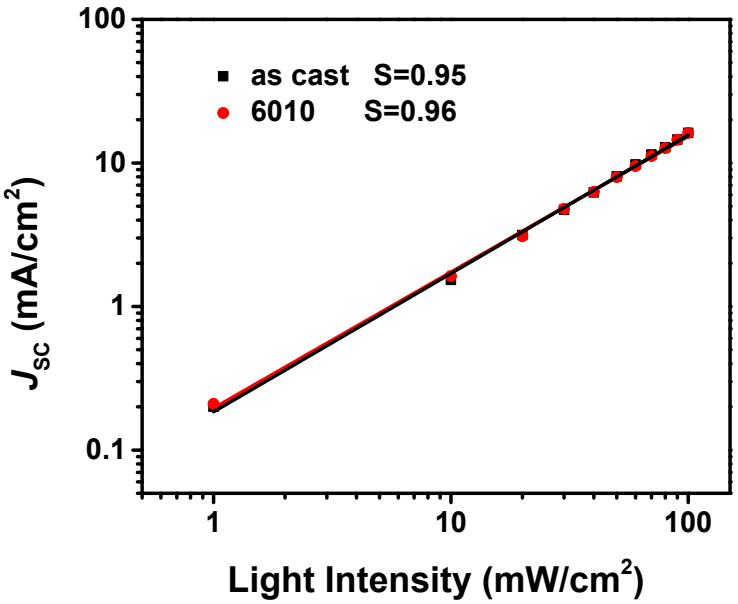

Fig. S9 The dependence of J_{sc} on light density with the corresponding fitting results for the PTB7-Th:**SF-4PDI2** -based devices (as-cast, annealed at 60 °C for 10 mins).

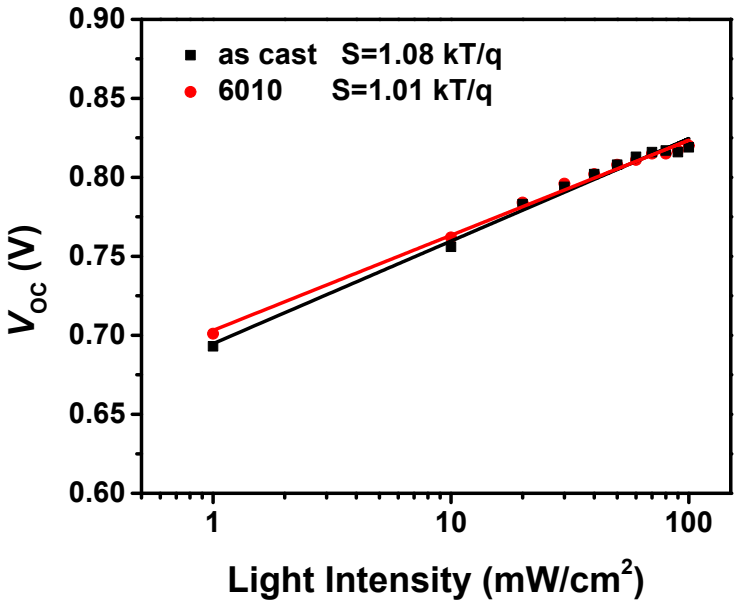

Fig S10 The dependence of V_{oc} on light density with the corresponding fitting results for the PTB7-Th:**SF-4PDI2** -based devices (as-cast, annealed at 60 °C for 10 mins).

11. Microscopic Morphology Characterizations

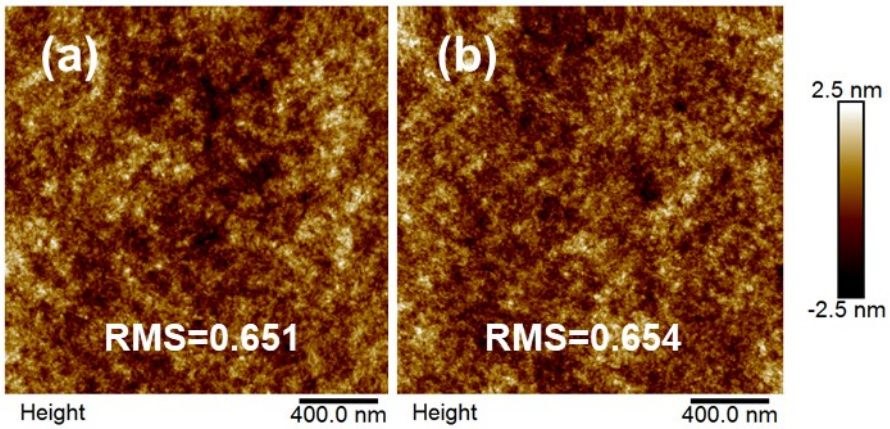

Fig. S11 The atomic force microscope (AFM) height images of PTB7-Th:**SF-4PDI2**, (a) as-cast film, (b) annealed films (annealed upon 60 °C for 10 min).

13. ^{1}H and ^{13}C NMR Spectra

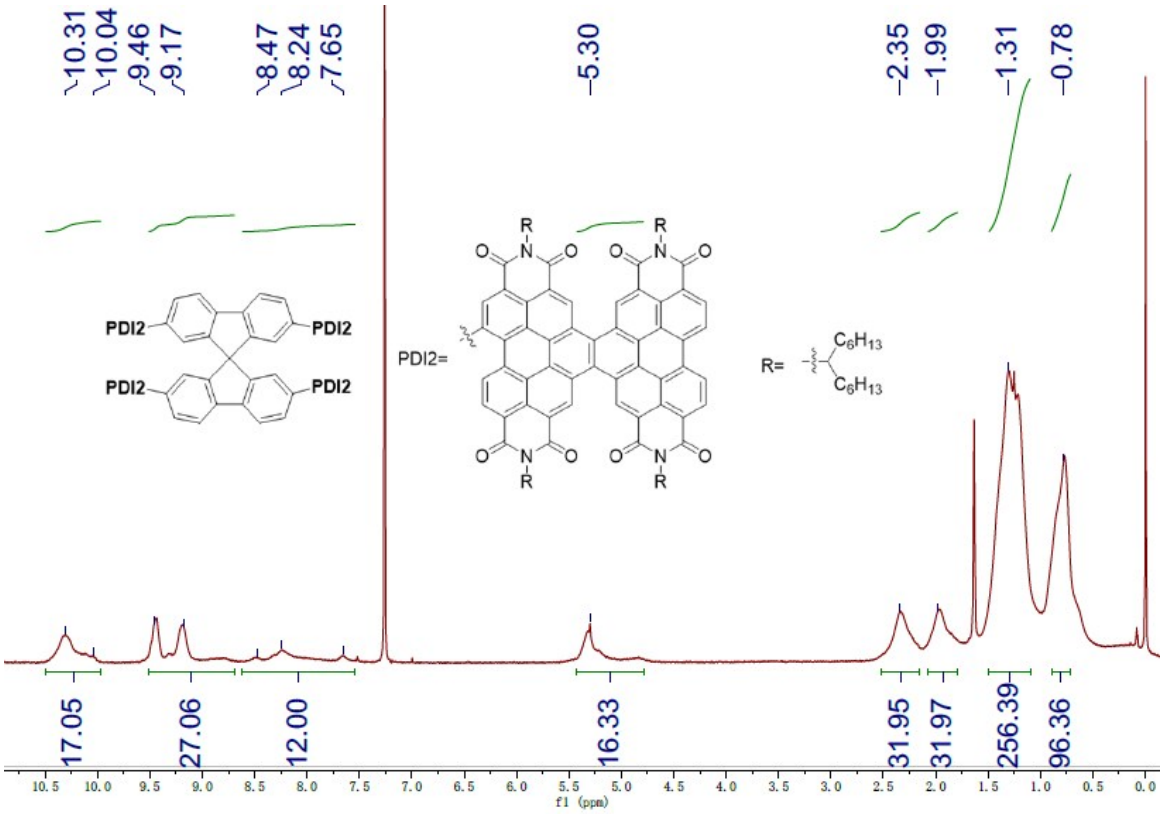

Fig. S12 ^{1}H NMR spectra of **SF-4PDI2**.

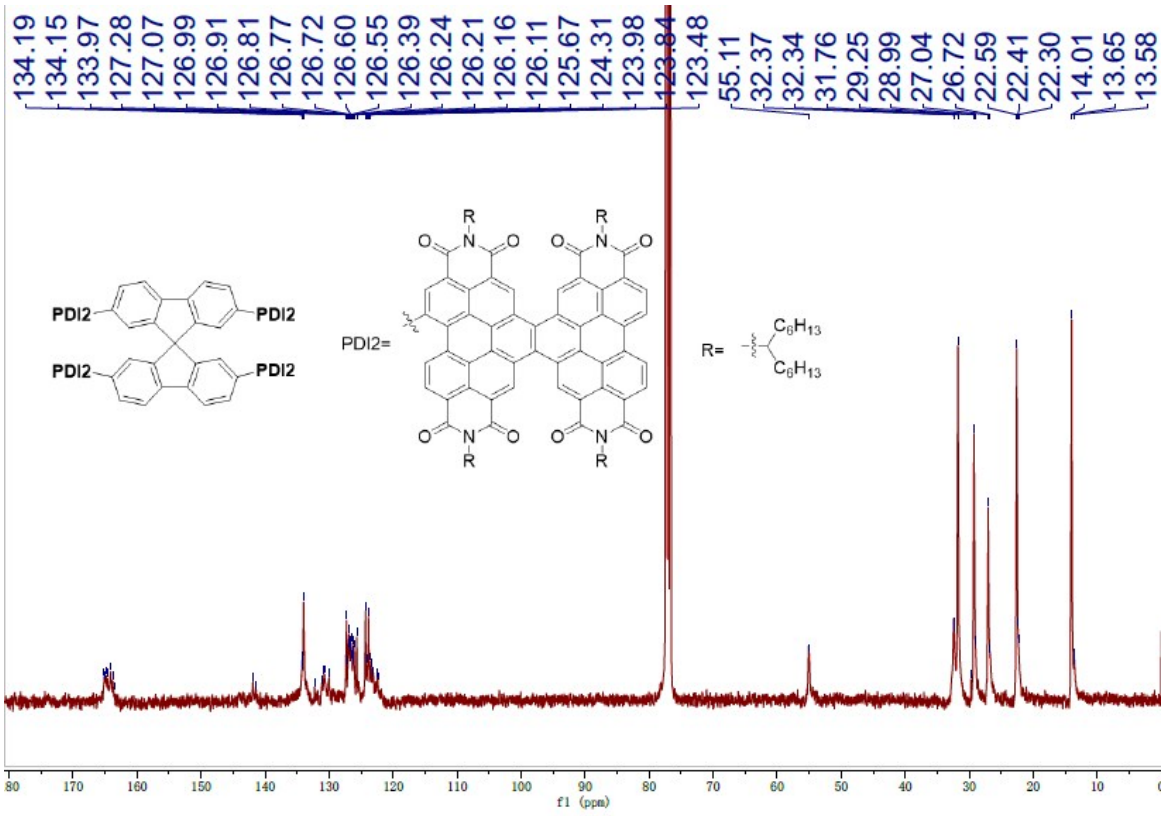

Fig. S13 ^{13}C NMR spectra of **SF-4PDI2**.

14.MALDI-TOF Mass Spectrum

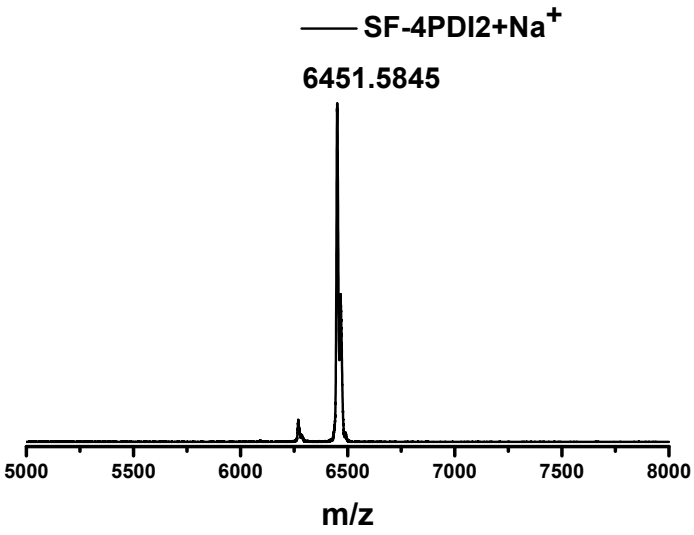

Fig. S14 MALDI-TOF Mass Spectrum for **SF-4PDI2**.

Notes and references

1. T. J. Sisto, Y. Zhong, B. Zhang, M. T. Trinh, K. Miyata, X. Zhong, X. Y. Zhu, M. L. Steigerwald, F. Ng and C. Nuckolls, *J. Am. Chem. Soc.*, 2017, **139**, 5648-5651.
2. A. Wicklein, A.Lang,, M. Muth and M. Thelakkat, *J. Am. Chem. Soc.*, 2009, **131**, 14442-14453.
3. P. Rajasingh, R. Cohen, E. Shirman, L. J. W. Shimon and B. Rybtchinski, *J. Org. Chem.*, 2007, **72**, 5973-5979.
4. Y. Zhong, M. T. Trinh, R. Chen, W. Wang, P. P. Khlyabich, B. Kumar, Q. Xu, C. Y. Nam, M. Y. Sfeir, C. Black, M. L. Steigerwald, Y. L. Loo, S. Xiao, F. Ng, X. Y. Zhu and C. Nuckolls,. *J. Am. Chem. Soc.*, 2014, **136**, 15215-15221.
5. T. Lu and F. Chen, *J. Comput. Chem.*, 2012, **33**, 580-592.
6. W. Humphrey, A. Dalke and K. Schulten, *J. Mol. Graphics*, 1996, **14**, 33-38.
7. J. Yi, Y. Wang, Q. Luo, Y. Lin, H. Tan, H. Wang and C. Q. Ma, *Chem. Commun.,* 2016, **52**, 1649-1652.
8. X Yi, B Gautam, I Constantinou, Y Cheng, Z Peng, E Klump, X Ba, C Ho, C Dong, S R. Marder, J R. Reynolds, S-W Tsang, H Ade and F. So, *Adv. Funct. Mater.,* 2018, **28**, 1802702.
9. R. Singh, J. Lee, M. Kim, P. E. Keivanidis and K. Cho, *J. Mater. Chem. A,* 2017, **5**, 210-220.
10. L. Yang, Y. Chen, S. Chen, T. Dong, W. Deng, L. Lv, S. Yang, H. Yan and H. Huang, *J. Power Sources,* 2016, **324**, 538-546.

11. K. C. Song, R. Singh, J. Lee, D. H. Sin, H. Lee and K. Cho, *J. Mater. Chem. C,* 2016, **4**, 10610-10615.

12. J. Lee, R. Singh, D. H. Sin, H. G. Kim, K. C. Song and K. Cho, *Adv. Mater.,* 2016, **28**, 69-76.

13. Z. Liu, L. Zhang, M. Shao, Y. Wu, D. Zeng, X. Cai, J. Duan, X. Zhang and X. Gao, *ACS Appl. Mater. Interfaces,* 2018, **10**, 762-768.

14. S. Jinnai, Y. Ie, Y. Kashimoto, H. Yoshida, M. Karakawa and Y. Aso, *J. Mater. Chem. A,* 2017, **5**, 3932-3938.

15. S. Chen, G. Zhang, J. Liu, H. Yao, J. Zhang, T. Ma, Z. Li and H. Yan, *Adv. Mater.,* 2017, **29**. 1604231

16. J. Zhao, Y. Li, H. Lin, Y. Liu, K. Jiang, C. Mu, T. Ma, J. Y. Lin Lai, H. Hu, D. Yu and H. Yan, *Energy Environ. Sci.,* 2015, **8**, 520-525.

17. Q. Yan, Y. Zhou, Y.-Q. Zheng, J. Pei and D. Zhao, *Chem. Sci*., 2013, **4**, 4389–4394

18. X. Zhou, Q. Sun, W. Li, Y. Zhao, Z. Luo, F. Zhang and C. Yang, *Dyes and Pigments,* 2017, **146**, 151-158.